

Image Segmentation Based on Oscillatory Correlation

DeLiang Wang[†] and David Terman[‡]

[†]Department of Computer and Information Science and Center for Cognitive Science

[‡]Department of Mathematics

The Ohio State University, Columbus, Ohio 43210, USA

Abstract

We study image segmentation on the basis of locally excitatory globally inhibitory oscillator networks (LEGION), whereby the phases of oscillators encode the binding of pixels. We introduce a lateral potential for each oscillator so that only those oscillators with strong connections from their neighborhood can develop high potentials. Based on the concept of the lateral potential, a solution to remove noisy regions in an image is proposed for LEGION, so that it suppresses the oscillators corresponding to noisy regions, without affecting those corresponding to major regions. We show that the resulting oscillator network separates an image into several major regions, plus a background consisting of all noisy regions, and illustrate network properties by computer simulation. The network exhibits a natural capacity in segmenting images. The oscillatory dynamics leads to a computer algorithm, which is applied successfully to segmenting real gray-level images. A number of issues regarding biological plausibility and perceptual organization are discussed. We argue that LEGION provides a novel and effective framework for image segmentation and figure-ground segregation.

1. Introduction

The segmentation of a visual scene (image) into a set of coherent patterns (objects) is a fundamental aspect of perception, which underlies a variety of tasks such as image processing, figure-ground segregation, and automatic target recognition. Scene segmentation plays a critical role in the understanding of natural scenes. Although humans perform it with apparent ease, the general problem of image segmentation remains unsolved in sensory information processing. As the technology of single-object recognition becomes more and more advanced in recent years, the demand for a solution to image segmentation is increasing since both natural scenes and manufacturing applications of computer vision are rarely composed of a single object.

Objects appear in a natural scene as the grouping of similar sensory features and the segregation of dissimilar ones. Sensory features are generally taken to be local, and in the simplest case may correspond to single pixels. To approach the problem of scene segmentation, three basic issues must be addressed: What are the cues that determine grouping and segregation? What is the proper representation for the result of segmentation? How are the cues used to give rise to segmentation?

Much is known about sensory cues that are important for segmentation. In particular, Gestalt psychology has uncovered a set of principles guiding the grouping process in the visual domain (Wertheimer 1923; Koffka 1935; Rock and Palmer 1990). These principles work together to produce segmentation. We briefly summarize some of the most important principles (see also Rock and Palmer 1990):

- *Proximity*. The closer the features lie to each other, the easier they are to be grouped into the same segment.
- *Similarity*. Features that have similar attributes, such as grayness, color, depth, texture, etc., tend to group together.
- *Common fate*. Features that have similar temporal behavior tend to group together. For instance, a group of features that move coherently (common motion) would form a single object. Notice that common fate may be regarded as one aspect of similarity. We list it separately to emphasize the importance of time as a separate dimension.
- *Connectedness*. A uniform, connected region, such as a spot, line, or more extended area, tends to form a single segment.
- *Good continuation*. A set of features that form a smooth and continuous curve tend to group together.
- *Prior knowledge*. If a set of features belong to the same familiar pattern, they tend to group together.

In computer vision algorithms for image segmentation, the result of segmentation can be represented in many ways. However, it is not a trivial task to represent the outcome of segmentation in a neural network. One proposal is naturally derived from the so-called *neuron doctrine* (Barlow 1972), where neurons at higher brain areas are assumed to become more selective and eventually a single neuron represents each single object (the grandmother-cell representation). Multiple objects in a visual scene would be represented by the coactivation of multiple units at some level of the nervous system. This representation faces major theoretical and neurobiological problems (von der Malsburg 1981; Abeles 1991; Singer 1993). Another proposal relies on *temporal correlation* to encode the binding (Milner 1974; von der Malsburg 1981; Abeles 1982). In particular, the correlation theory of von der Malsburg (1981) asserts that an object is represented by the temporal correlation of the firing activities of the scattered cells that encode different features of the object. Multiple objects are represented by different correlated firing patterns that alternate in time, each corresponding to a single object.

Temporal correlation provides an elegant way to represent the result of segmentation. A special form of temporal correlation is *oscillatory correlation*, where the basic unit is a neural oscillator (see Terman and Wang 1995; Wang and Terman 1995a). However, this representation does not, by itself, reveal *how* segmentation is achieved using Gestalt grouping principles. Despite an extensive body of literature dealing with segmentation using temporal correlation (starting perhaps from von der Malsburg and Schneider 1986), little progress has been made in building successful neural systems for image segmentation. There are two major challenges facing the oscillatory correlation theory. The first challenge is how to achieve fast synchronization within a population of locally coupled oscillators. Most of the models proposed for achieving phase synchrony rely on all-to-all connections (see Sect. 2 for more details). However, as pointed out by Sporns et al. (1991) and Wang (1993a), a network with full connections indiscriminately connects all the oscillators which are activated simultaneously by different objects, because the network is dimensionless and loses critical information about geometry. The second challenge is how to achieve fast desynchronization among different groups of oscillators representing distinct objects. This is necessary in order to segment multiple objects simultaneously presented.

We have previously proposed a neural network framework to deal with the problem of image segmentation, called Locally Excitatory Globally Inhibitory Oscillator Networks (LEGION) (Wang and Terman 1995a; Terman and Wang 1995). Each oscillator is modeled as a standard relaxation oscillator. Local excitation is implemented by positive coupling between neighboring oscillators and global inhibition is realized by a global inhibitor. LEGION exhibits the mechanism of *selective gating*, whereby oscillators stimulated by the same pattern tend to synchronize due to local excitation and oscillator groups stimulated by different patterns tend to desynchronize due to global inhibition (Wang and Terman 1995a; Terman and Wang 1995). We have proven that, with the selective gating mechanism, LEGION rapidly achieves both synchronization within groups of

oscillators that are stimulated by connected regions and desynchronization between different groups. In sum, LEGION provides an elegant solution to both challenges outlined above.

In this paper, we study LEGION for segmenting real images. Before we demonstrate image segmentation, the original version of LEGION needs to be extended to handle images with many tiny (noisy) regions. One such example is shown in Fig. 1, where three objects with a noisy background form a visual image. Without extension, LEGION would treat each region, no matter how small it is, as a separate segment. Thus, it would lead to many tiny fragments. We call this problem *fragmentation*. A more serious problem is that it is difficult to choose parameters so that LEGION is able to achieve more than several (5 to 10) segments (Terman and Wang 1995). Noisy fragments may, therefore, compete with major image regions for becoming segments, so that it may not be possible to extract the major segments from an image. The problem of fragmentation is solved by introducing a concept of lateral potential for each oscillator. The extended dynamics is fully analyzed (Wang and Terman, 1996), and the resulting LEGION network is applied to gray-level images and yields successful segmentation. A preliminary version of this work was presented in Wang and Terman (1995b).

In the next section we review prior work relevant to image segmentation and neural networks. In Section 3, our model is described in detail. In Section 4, computer simulations of the extended LEGION network are presented. Section 5 presents the segmentation results on real images. Further discussions concerning our approach are given in Section 6.

2. Related Work

2.1 Image Segmentation Algorithms

Due to its critical importance for computer vision, image segmentation has been studied extensively. Many techniques have been invented (for reviews of the subject see Zucker 1976; Haralick 1979; Haralick and Shapiro 1985; Sarkar and Boyer 1993b). Broadly speaking, there are three categories of algorithms: pixel classification, edge-based organization, or region-based segmentation. A simple classification technique is thresholding: a pixel is assigned a specific label if some measure of the pixel passes a certain threshold. This idea can be extended to a complex form including multiple thresholds which are determined by pixel histograms (Kohler 1981). Edge-based techniques generally start with an edge-detection algorithm, which is followed by grouping edge elements into rectilinear or curvilinear lines. These lines are then grouped into boundaries that can be used to segment images into various regions (see, for example, Geman *et al.* 1990; Sarkar and Boyer 1993a; Foresti *et al.* 1994). Finally, region-based techniques operate directly on regions. A classical method is region growing/splitting (or split-and-merge, see Horowitz and Pavlidis 1976; Zucker 1976; Adams and Bischof 1994), where iterative steps are taken to grow (split) pixels into a connected region if all the pixels in the region satisfy some conditions. One of the apparent deficits with these algorithms is their iterative (serial) nature (Liou *et al.* 1991). There are some recent algorithms which are partially parallel (Liou *et al.* 1991; Mohan and Nevatia 1992; and Manjunath and Chellappa 1993).

Most of these techniques rely on domain-specific heuristics to perform segmentation, and no unified computational framework exists to explain the general phenomenon of scene segmentation (Haralick and Shapiro 1985). The problem of scene segmentation is computationally hard (Gurari and Wechsler 1982), and largely regarded unsolved.

2.2 Neural Network Efforts

Neural networks have proven to be a successful approach to pattern recognition (Schalkoff 1992; Wang 1993b). Unfortunately, little work has been devoted to scene segmentation which is generally regarded as part of preprocessing (often meaning manual segmentation). Scene segmentation is a particularly challenging task for neural networks, partly because traditional neural

networks lack the representational power for encoding multiple objects simultaneously. Interesting schemes of segmentation based on learning have been proposed before (Sejnowski and Hinton 1987; Mozer *et al.* 1992). Grossberg and Wyse (1991) proposed a model for segmentation based on the contour detection model of Grossberg and Mingolla (1985; see Gove *et al.* in press for a computer simulation). However, all of these methods were tested only on small synthetic images, and it is not clear how they can be extended to handle real images. Also, Kohonen's self-organizing maps have been used for segmentation based on pixel classification (Kohonen 1995; Koh *et al.* 1995). A primary drawback of these methods is that the number of segments (objects) is assumed to be known *a priori*.

Because temporal (oscillatory) correlation offers an elegant way of representing multiple objects in neural networks (von der Malsburg and Schneider 1986), most of the neural network efforts on image segmentation have centered around this theme. In particular, the discovery of synchronous oscillations in the visual cortex has triggered much interest in exploring oscillatory correlation to solve the problems of segmentation and figure-ground segregation. One type of model uses all-to-all connections to reach synchronization (Wang *et al.* 1990; Sompolinsky *et al.* 1991; von der Malsburg and Buhmann 1992). As explained in Sect. 1, these models cannot extend very far in solving the segmentation problem because fundamental information concerning the geometry among sensory features is lost. Another type of model uses lateral connections to reach synchrony (Sporns *et al.* 1991; Murata and Shimizu 1993; Schillen and König 1994). Unfortunately, it is unclear to what extent these oscillator networks can synchronize on the basis of local connectivity since no analysis is given and only simulation results on small networks are provided. Moreover, recent insights into the contrasting behavior between sinusoidal and relaxation oscillators makes clear that sinusoid-typed oscillators, which encompass most of the oscillator models used, have severe limitations to support fast synchronization (Wang 1995; Terman and Wang 1995; Somers and Kopell in press). In fact, in all of the above models, nothing close to a real image has ever been used for testing these models.

3. Model Description

The building block of LEGION, a single oscillator i , is defined as a feedback loop between an excitatory unit x_i and an inhibitory unit y_i , whose time derivatives are defined as

$$x_i' = 3x_i - x_i^3 + 2 - y_i + I_i H(p_i + \exp(-\alpha t) - \theta) + S_i + \rho \quad (1a)$$

$$y_i' = \varepsilon (\gamma(1 + \tanh(x_i/\beta)) - y_i) \quad (1b)$$

Here H stands for the Heaviside step function, which is defined as $H(v) = 1$ if $v \geq 0$ and $H(v) = 0$ if $v < 0$. I_i represent external stimulation which is assumed to be applied from time 0 on, and S_i denotes the coupling from other oscillators in the network. ρ denotes the amplitude of Gaussian noise, the mean of which is set to $-\rho$. The negative mean is used to reduce the chance of self-generating oscillations, which will become clear in the next paragraph. The noise term is introduced for two purposes. The first one is obvious: to test the robustness of the system. The second one, perhaps more important, is to play an active role in separating different input patterns (for more discussions see Terman and Wang 1995).

The parameter ε is a small positive number. Hence (1), without any coupling or noise and with constant stimulation, corresponds to a standard relaxation oscillator. The x -nullcline of (1) is a cubic curve, while the y -nullcline is a sigmoid function. If $I > 0$ and $H = 1$, these curves intersect along the middle branch of the cubic when β is small. In this case, we call the oscillator *enabled* (see Fig. 2A). It produces a stable periodic orbit, which alternates between *silent* and

active phases of near steady-state behavior. As shown in Fig. 2A, the silent and the active phases correspond to the left L and the right R branches of the cubic, respectively. The transitions between the two phases occur rapidly (thus referred to as *jumping*). Notice that the trajectory of the oscillator in phase space jumps between the two branches and then follows closely the branches, because the small ε induces very different time scales for x - and y -dynamics. The parameter γ is used to control the ratio of the times that the solution spends in these two phases. For a larger value of γ , the solution spends a shorter time in the active phase. If $I \leq 0$ and $H = 1$, the nullclines of (1) intersect at a stable fixed point along the left branch of the cubic (see Fig. 2B). In this case (1) produces no periodic orbit, and the oscillator is referred to as *excitable*, indicating the oscillator has not yet been but can be excited by stimulation. An excitable oscillator may become oscillatory if it receives, through the term S , large enough coupling from other oscillators. Because of this dependency on external stimulation, the oscillations are stimulus-dependent. We say that the oscillator is *stimulated* if $I > 0$, and *unstimulated* if $I \leq 0$. The parameter β specifies the steepness of the sigmoid function, and is chosen to be small. The oscillator model (1) may be interpreted as a model for the spiking behavior of a single neuron, the envelope of a bursting neuron, or a mean field approximation to a network of excitatory and inhibitory binary neurons.

The primary difference between (1) and the model in Terman and Wang (1995) is the introduction of the Heaviside function in which $\alpha > 0$ and $0 < \theta < 1$. The parameter α is chosen to be on the same order of magnitude as ε so that the exponential function decays on a slow time scale. It is the Heaviside term which allows the network to distinguish between major blocks and noisy fragments. The basic idea is that a major block must contain at least one oscillator, denoted as a *leader*, which lies in the center of a large homogeneous region. This oscillator will be able to receive large lateral excitation from its neighborhood. A noisy fragment does not contain such an oscillator. The variable p_i in (1a) determines whether or not an oscillator is a leader. It is referred to as the *lateral potential* of the oscillator i , and satisfies the differential equation:

$$p_i' = \lambda (1 - p_i) H\left[\sum_{k \in N(i)} T_{ik} H(x_k - \theta_x) - \theta_p\right] - \mu p_i \quad (2)$$

Here $\lambda > 0$, T_{ik} is the *permanent* connection weight (explained later) from oscillator k to i , and $N(i)$ is called the *neighborhood* of i . If the weighted sum oscillator i receives from $N(i)$ exceeds the threshold θ_p , p_i approaches 1. If this weighted sum is below θ_p , p_i relaxes to 0 on a time scale determined by μ , which is chosen to be on the same order as ε resulting in a slow time scale. It follows that p_i can only exceed the threshold θ in (1a) if i is able to receive a large enough lateral excitation from its neighborhood. In order to develop a high potential, it is not sufficient that a large number of neighbors of i are oscillatory. They must also have a certain degree of synchrony in their oscillations. In particular, they must all exceed the threshold θ_x at the same time in their oscillations.

The purpose of introducing the lateral potential is that an oscillator with a high potential can *lead* the activation of an oscillator block corresponding to an object. Though a high-potential oscillator need not be stimulated, it must be stimulated, however, in order to play the role of leading an oscillator block; otherwise, the oscillator will not oscillate at all. Thus, we require that a leader be always stimulated. More formally, an oscillator i is defined as a leader if $p_i \geq \theta$ and i is stimulated. The lateral potential of every oscillator is initialized to zero.

The network we study for image segmentation is two dimensional. Figure 3 shows the simplest case of permanent connectivity, where an oscillator is connected only with its four immediate neighbors except on the boundaries where no wrap-around is used. Such connectivity forms a 2-D grid. In general, however, $N(i)$ should be larger, and the permanent connection weights should take on the form of a Gaussian distribution with their distance.

The coupling term S_i in (1) is given by

$$S_i = \sum_{k \in N(i)} W_{ik} H(x_k - \theta_x) - W_z H(z - \theta_{xz}) \quad (3)$$

where W_{ik} is the *dynamic* connection weight from k to i . The neighborhood of the above summation is chosen to be the same as (2). In some situations, however, they should be chosen differently to achieve good results, and an alternative definition with two different neighborhoods is given elsewhere (Wang and Terman 1996).

Now let us explain permanent and dynamic connection weights. To facilitate synchrony and desynchrony (more discussions later), we assume that there are two kinds of synaptic weights (links) between two oscillators following von der Malsburg who argued for its neurobiological plausibility (von der Malsburg 1981; von der Malsburg and Schneider 1986; see also Crick 1984). The permanent weight, or T_{ik} , embodies the hardwired structure of a network. On the other hand, the dynamic weight, or W_{ik} , rapidly changes. W_{ik} is formed on the basis of T_{ik} according to the mechanism of dynamic normalization (Wang 1995). Dynamic normalization was previously defined as a two-step procedure: First update dynamic links and then normalization (Wang 1995; Terman and Wang 1995). There are different ways to realize such normalization. In the following, we give one way to implement dynamic normalization in differential equations,

$$u'_i = \eta (1 - u_i) I_i - \nu u_i \quad (4a)$$

$$W'_{ik} = W_T T_{ik} u_i u_k - W_{ik} \sum_{j \in N(i)} T_{ij} u_i u_j \quad (4b)$$

The function u_i measures whether oscillator i is stimulated, and it is initialized to 0. The parameter η determines the rate of updating u_i . When $I_i > 0$, $u_i \rightarrow 1$ quickly because we choose $\eta \gg \nu$ (see below); otherwise when $I_i = 0$, $u_i = 0$. For this equation we assume $I_i = 0$ if oscillator i is unstimulated (otherwise it is easy to enforce this by applying a step function on I_i). The parameter ν is chosen to be on the same order as ε , so that u_i slowly relaxes back to 0 after the external stimulus is withdrawn.

We assume that W_{ik} are initialized to 0 for all i and k . It is easy to see that if oscillator i is unstimulated, W_{ik} remains to be 0 for all k , and if oscillator k is unstimulated $W_{ik} = 0$ for all i . Otherwise, if $u_i = 1$ and $u_k = 1$ for at least one $k \in N(i)$, then at equilibrium,

$$W_{ik} = \frac{W_T T_{ik} u_i u_k}{\sum_{j \in N(i)} T_{ij} u_i u_j} \quad \text{and} \quad \sum_{k \in N(i)} W_{ik} = W_T$$

Thus the total dynamic weights converging to a single oscillator equals W_T , which gives the desired normalization. Notice that dynamic weights, not permanent weights, participate in determining S_i (see (3)). Moreover, W_{ik} can be properly set up in one step at the beginning based on external stimulation, which should be useful for engineering applications.

It should be mentioned that weight normalization is not a necessary condition for the selective gating mechanism to work. This conclusion has been established previously (Terman and Wang 1995). With normalized weights, however, the quality of synchronization within each oscillator block is better (Terman and Wang 1995).

In (3), W_z is the weight of inhibition from the global inhibitor z , whose activity, also denoted by z , is defined as

$$z' = \phi(\sigma_\infty - z) \quad (5)$$

where $\sigma_\infty = 1$ if $x_i \geq \theta_{zx}$ for at least one oscillator i , and $\sigma_\infty = 0$ otherwise. Hence θ_{zx} represents another threshold, and it is chosen so that only an oscillator jumping to the active phase can trigger the global inhibitor. If σ_∞ equals 1, $z \rightarrow 1$. The parameter ϕ represents the rate at which the inhibitor reacts to the stimulation from the oscillator network.

The introduction of a lateral potential provides a solution to the problem of fragmentation. There is an initial period when the term $\exp(\alpha t)$ exceeds the threshold θ . During this period, every stimulated oscillator is enabled. This allows the leaders to receive sufficient lateral excitation so that they can achieve a high potential. After this initial period, the only oscillators which can jump up without stimulation from other oscillators are the leaders. When a leader jumps up, it spreads its activity to other oscillators within its own block, so they can also jump up. These oscillators are referred to as *followers*. Oscillators not in this block are prevented from jumping up, because of the global inhibitor. The oscillators which belong to the noisy fragments will not be able to jump up beyond the initial period, because these oscillators will not be able to develop a sufficiently high potential by themselves and they cannot be recruited by leaders. These oscillators are referred to as *loners*. In order to be oscillatory beyond the initial time period, an oscillator must either be a leader or a follower. This indicates that the oscillator is not part of a noisy fragment, because noisy fragments in an image tend to be small and isolated (see Fig. 1). The collection of all noisy regions whose corresponding oscillators are loners is called the *background*, which is not a uniform region and generally discontinuous.

We have proven a number of rigorous results concerning the system (1)-(5). Our main result implies that the loners will no longer be able to oscillate after an initial time period. Moreover, the asymptotic behavior of a leader or a follower is precisely the same as the network obtained by simply removing all the loners. Together with the results in Terman and Wang (1995), this implies that after a number of oscillation cycles a block of oscillators corresponding to a single major image region will oscillate in synchrony, while any two oscillator blocks corresponding to two major regions will desynchronize from each other. Also, the number of cycles required for full segmentation is no greater than the number of major regions plus one. The details of the analysis are given in Wang and Terman (1996).

The analysis in Wang and Terman (1996) is constructive in the sense that it leads to precise estimates that the parameters must satisfy. It shows that the results hold for a robust range of parameter values. Moreover, the analysis does not depend on the precise form of nonlinear functions in (1). The specific cubic and sigmoid functions (see Fig. 2) are used because of their simplicity. In addition to the parameter description given earlier, we require that $0 < \theta < 1$, and α be chosen so that all the stimulated oscillators remain enabled for the first cycle, but only leaders remain enabled during the second cycle. In (2), we simply require that λ be on the same order of magnitude as 1, and $0 < \theta_p < 1$. The parameter η in (4) simply needs to be on the same order of 1.

There are alternative ways of defining the model without affecting its essential dynamics (Wang and Terman 1996). In particular, we have given a definition where dynamic normalization of connection strengths in (4) is not needed, but the quality of synchrony within each block and the flexibility for choosing parameters seem somewhat lessened.

4. Computer Simulation

To illustrate how the LEGION network is used for image segmentation while eliminating fragmentation, we have simulated a 50x50 grid of oscillators with a global inhibitor as defined by (1)-(5). We map the three objects (designated as the *sun*, a *tree*, and a *mountain*) in Fig. 1, and then add 20% noise so that each uncovered square has a 20% chance of being covered (stimulated). The resulting image is shown in Fig. 4A. In the simulation, $N(i)$ is simply the four nearest-neighbors without boundary wrap-around. For all the stimulated oscillators $I = 0.2$, while for the others $I = 0$. Notice that if oscillator i is unstimulated, $W_{ik} = W_{ki} = 0$ for all k , and I_i does not need to be negative to prevent i from oscillating. The amplitude ρ of the Gaussian noise was set to 0.02. This represents a 10% noise level compared to the external stimulation. We observed during the simulations that noise facilitated the process of desynchronization.

The differential equations (1)-(5) were solved using both a fourth-order Runge-Kutta method and the adaptive grid o.d.e. solver LSODE. Permanent connections between any two neighboring oscillators were set to 2.0, and for total dynamic connections (see (4b)), $W_T = 8.0$. Dynamic weights W_{ik} were set up at the beginning according to (4). The following values for the other parameters in (1)-(5) were used: $\varepsilon = 0.02$, $\alpha = 0.005$, $\beta = 0.1$, $\gamma = 6.0$, $\theta = 0.9$, $\lambda = 0.1$, $\theta_x = -0.5$, $\theta_p = 7.0$, $W_z = 1.5$, $\eta = 1.0$, $\mu = \nu = 0.01$, $\phi = 3.0$, and $\theta_{zx} = \theta_{xz} = 0.1$. The value of θ_p was chosen so that, in order to achieve a high potential, an oscillator must have all of four neighbors active. The simulation results were robust to considerable changes in the parameter values. Fig. 4B-4E show the instantaneous activity (snapshot) of the network at various stages of dynamic evolution. The diameter of each black circle represents the x activity of the corresponding oscillator. Specifically, if the range of x values of all the oscillators is given by x_{min} and x_{max} , then the diameter of the black circle corresponding to one oscillator is set to be proportional to $(x - x_{min}) / (x_{max} - x_{min})$.

Fig. 4B shows the snapshot at the beginning of the dynamic evolution. This is included to illustrate the random initial conditions. Fig. 4C shows a snapshot shortly after Fig. 4Bz. One can clearly see the effect of synchrony and desynchrony: all the stimulated oscillators which belong to or are the neighbors of the *sun* are entrained and have large activities (in the active phase). At the same time, the oscillators stimulated by the rest of the image have very small activities (in the silent phase). Thus the noisy *sun* is segmented from the rest of the image. A short time later, as shown in Fig. 4D, the oscillators in the group representing the noisy *tree* reach their active phase and are separated from the rest of the image. Fig. 4E shows another snapshot, when the noisy *mountain* has its turn to be activated and separate from the rest of the input. This successive "pop-out" of the segments continues in a stable periodic fashion until the input image is withdrawn. To illustrate the entire segmentation process, Figure 5 shows the temporal evolution of every stimulated oscillator. The activities of the oscillators stimulated by each noisy object are combined together as one trace in the figure, and so are for the background. Since the oscillators receiving no external stimulation remain excitable and unable to oscillate throughout the simulation process, they are excluded from the display. The three upper traces represent the activities of the three oscillator blocks, and the fourth one represents the background consisting of all of the scattered dots. Because of low potentials, these oscillators quickly become excitable even though they are enabled at the beginning. The bottom trace represents the activity of the global inhibitor. The synchrony within each block and desynchrony between different blocks are clearly shown after three cycles.

To illustrate the role of the lateral potential, the same network with the same input (Fig. 4A) and the same initial condition has been simulated without the lateral potential. In this case, the Heaviside function in (1a) is always 1 for every oscillator. With the random initial condition shown in Fig. 4F, the network reaches a stable oscillatory behavior with four segments, after less than three cycles. The four segments are shown in Fig. 4G-4J. Without the lateral potential, the network cannot distinguish major image regions from noisy fragments and separate major regions apart.

With a fixed set of parameters, the dynamical system of LEGION can segment only a limited number of patterns. This number depends, to a large extent, on the ratio of the times that a single

oscillator spends in the silent and active phases. Let us refer to this limit as the *segmentation capacity* of LEGION. In the above simulation, the number of the major blocks to be segmented is within the segmentation capacity. What happens if this number exceeds the segmentation capacity? From the analysis in Wang and Terman (1996), we know that the system will separate the entire image into as many segments as the capacity allows, where each segment may correspond to one major block (called *simple segment*) or a number of major blocks (called *congregate segment*). To illustrate this point, we show the following simulation, where we present to a 30x30 LEGION network with an arbitrary image containing nine binary patterns, which together form the phrase **OHIO STATE** as shown in Fig. 6A. We then add 10% random noise to the input in a similar way as in Fig. 4, resulting in Fig. 6B. We use the same parameter values as in the simulations presented in Fig. 4, except that $\gamma = 8.0$. For this set of parameters, our earlier experiments showed that the system's segmentation capacity is less than 9. The simulation results are presented in Fig. 6C-6H. Shortly after the start of system evolution, the LEGION network segmented the input of Fig. 6B into five segments, shown in Fig. 6D-6H respectively. Among these five segments, three are simple segments (Fig. 6D, 6E, and 6H) and two are congregate segments (Figs. 6F and 6G). Besides Fig. 6, many other simulations have been performed for the input of Fig. 6B with different random initial conditions, and the results are comparable with Fig. 6. There are different ways, however, that the system separates the nine noisy patterns into five segments. For this particular set of parameters, the segmentation capacity of the LEGION network is 5. In fact, we have not seen a single simulation trial where more than 5 segments are produced. This important property of the system, i.e. it naturally exhibits a segmentation capacity, is in good accord with the well-known psychological principle that there are fundamental limits on the number of simultaneously perceived objects.

5. Real Images

LEGION can segment gray-level images in a way similar to segmenting binary images. For a given image, a LEGION network of the same size as the image with a global inhibitor is used to perform segmentation. Each pixel of the image corresponds to an oscillator of the network, and we assume that every oscillator is stimulated when the image is applied to the network. The main difference between gray-level and binary images lies in how to set up connections. For gray-level images, the coupling strength between two neighboring oscillators is determined by the similarity of two corresponding pixels. This simple way of setting up the coupling strength addresses only the grouping principles of proximity, connectedness, and similarity (cf. Sect. 1).

5.1 Algorithm

To segment real images with large numbers of pixels involves integrating a large number of the differential equations of (1)-(5). To reduce numerical computations on a serial computer, an algorithm is extracted from these equations. The algorithm follows major steps in the numerical simulation of the equations, and it exhibits the essential properties of relaxation oscillators, such as two time scales (fast and slow) and the properties of synchrony and desynchrony in a population of oscillators. Such extraction is quite straightforward because, in a relaxation oscillator network, much of the dynamics takes place when oscillators are jumping up or jumping down. Besides, the algorithm overcomes the segmentation capacity, which may be desired in some applications. More specifically, the following approximations have been made.

- (a) When no oscillator is in the active phase (see Fig. 2), the leader closest to the jumping point (left knee) among all enabled oscillators is selected to jump up to the active phase.
- (b) An oscillator takes one time step to jump up to the active phase if the net input it receives from neighboring oscillators and the global inhibitor is positive.
- (c) The alternation between the active phase and the silent phase of a single oscillator takes one time step only.

(d) All of the oscillators in the active phase jump down if no more oscillators can jump up. This situation occurs when the oscillators stimulated by the same pattern have all jumped up.

LEGION algorithm

Only the x value of oscillator i , x_i , is used in the algorithm. $N(i)$ is assumed to be the eight nearest neighbors of i without wrap-around. LK_x , RK_x , LC_x represent the x values of three of four corner points of a typical limit cycle (see Fig. 2A), where LC denotes the (upper) left corner of the limit cycle. By straightforward calculations, we obtain $LK_x = -1$, $LC_x = -2$, $RK_x = 1$. In the algorithm, I_i indicates the value of pixel i , and I_M indicates the maximum possible pixel value.

1. Initialize

1.1 Set $z(0) = 0$;

1.2 Form effective connections

$$w_{ij} = I_M / (1 + |I_i - I_k|), \quad k \in N(i)$$

1.3 Find leaders

$$p_i = H\left[\sum_{k \in N(i)} w_{ik} - \theta_p\right]$$

1.4 Place all the oscillators randomly on the left branch. Namely $x_i(0)$ takes a random value between LC_x and LK_x .

2. Find one oscillator j so that (1) $x_j(t) \geq x_k(t)$, where k is currently on the left branch; (2) $p_j = 1$. Then

$$x_j(t+1) = RK_x; \quad z(t+1) = 1 \quad \{\text{jump up}\}$$

$$x_k(t+1) = x_k(t) + (LK_x - x_j(t)), \quad \text{for } k \neq j.$$

In this step, the leader on the left branch which is closest to the left knee is selected. This leader jumps up to the right branch, and all the other oscillators move towards LK .

3. Iterate until stop

If ($x_i(t) = RK_x$ and $z(t) > z(t-1)$)

$$x_i(t+1) = x_i(t) \quad \{\text{stay on the right branch}\}$$

else if ($x_i(t) = RK_x$ and $z(t) \leq z(t-1)$)

$$x_i(t) = LC_x; \quad z(t+1) = z(t) - 1 \quad \{\text{jump down}\}$$

If ($z(t+1) = 0$) go to step 2

else

$$S_i(t+1) = \sum_{k \in N(i)} w_{ik} H(x_k(t) - LK_x) - w_z H(z(t) - 0.5)$$

If ($S_i(t+1) > 0$)

$$x_i(t+1) = RK_x; \quad z(t+1) = z(t) + 1 \quad \{\text{jump up}\}$$

else

$$x_i(t+1) = x_i(t) \quad \{\text{stay on the left branch}\}$$

Comparing the above algorithm with the dynamical system of (1)-(5), one can find the following simplifications.

(a) The dynamic weight W_{ij} is directly set to $W_{ij} = I_M/(1 + |I_i - I_k|)$. The intuitive reason for this choice of weights is that the more pixel i and pixel j are similar to each other, the stronger the connection between the two corresponding oscillators. It is worth noting that the algorithm does not compute normalized weights. As mentioned in Sect. 3, selective gating can still take place with this weight setting, even though the weights are not normalized.

(b) The leaders are chosen during initialization. According to the dynamics described in Sect. 3, lateral potentials, and thus leaders, are determined during a few initial cycles of oscillatory dynamics. Since every oscillator is stimulated, and W_{ij} is set at the beginning, it can be precisely predicted at the beginning which oscillators will become leaders. Thus, to save computational time, the leaders are determined in the initialization step. It should be clear that the number of leaders determined in this step does not correspond to the number of resulting segments - a major image region (segment) may generate many leaders.

There are two critical parameters in the algorithm: W_z and θ_p , where the former is the strength of global inhibition and the latter is the threshold for forming high potentials (leaders). For W_z , higher values make the algorithm more difficult to group pixels into regions. Thus, in order for a region to be grouped together, the algorithm demands a higher degree of homogeneity within the region. Generally speaking, given a gray-level image, higher W_z leads to more and smaller regions. For θ_p , higher values make the algorithm more difficult to develop leaders. Thus fewer leaders will be developed, and fewer regions result from the algorithm. On the other hand, regions produced with a higher θ_p tend to be more homogeneous. For image segmentation applications, it suffices to stop the algorithm when every leader has jumped up once. See Wang and Terman (1996) for some discussions on the algorithm.

5.2 Segmenting Real Images

5.2.1 Sum vs. Max: an aerial image

The first image the algorithm is tested on is an aerial image, called Lake, which is shown in Fig. 7A. As in the following images to be used, this is a typical gray-level image, where each pixel is an 8-bit number ranging from 0 to 255 (also called intensity), and pixels with higher values appear brighter. The image has 160x160 pixels, and is presented to a LEGION network of 160x160 oscillators. For this simulation, $W_z = 40$ and $\theta_p = 1200$. Quickly after the image is presented, the algorithm produces different segments at different time steps. Fig. 7B-7G display the first six segments that have been produced sequentially, where a black pixel corresponds to an oscillator in the active phase and a blank pixel corresponds to an oscillator in the silent phase. As shown in the figure, each segment corresponds to a meaningful region in the original image: a segment is either a lake, a field, or a parkway. The region in Fig. 7B corresponds to a lake. The region in Fig. 7C corresponds to the main lake, except for the lower-left part and on the right side where the lake region extends to non-lake parts. The parkway segment in Fig. 7G picks up a partial parkway network in the original image. The other segments match well with the fields of the image.

The entire image is separated into 16 regions and a background. To simplify the display, we put all the segments and the background together into one figure, using gray levels to indicate the phases of oscillator blocks. Such a display is called a *gray map*. The gray map of the results of this simulation is shown in Fig. 8A, where the background is shown by the black scattered areas.

Generally speaking, the background corresponds to parts of the image that have high intensity variations. Due to the mechanism of fragment removal, these noisy regions stay in the background, as opposed to many segments that would have been the result without fragment removal.

In the above algorithm, an oscillator summates all the input from its neighborhood, and if the overall input is greater than the global inhibition the oscillator jumps to the active phase (see also (3)). Another reasonable way of grouping is to replace summation by maximization when computing S_i :

$$S_i = \text{Max}_{k \in N(i)} \{W_{ik} H(x_k - \theta_x)\} - W_z H(z - \theta_{xz}) \quad (6)$$

Intuitively, the maximum operation concentrates on the relation of i with the oscillator in $N(i)$ that has the strongest coupling with i , but omits the relation between i and $N(i)$ as a whole. Thus, grouping by maximization emphasizes pairwise pixel relations, whereas grouping by summation emphasizes pixel relations in a local field.

By using (6) in the LEGION algorithm, the Lake image is segmented again. In this simulation, $W_z = 20$ and $\theta_p = 1200$. Fig. 8B shows the result of segmentation by a gray map. The entire image is segmented into 17 regions and a background, which is indicated by black areas. Each segment corresponds well with a relatively homogeneous region in the image. Interestingly, except for the parkway region in the lower part of the image, every region in Fig. 8B has a corresponding one in Fig. 8A. A comparison between the two figures reveals the difference between summation and maximization in segmentation. A closer comparison, however, indicates that the maximum scheme yields a little more faithful regions. On the other hand, regions in Fig. 8A appear smoother and have fewer "black holes" - parts of the background. The smoothing effect of summation is generally positive, but it may lose important details. For example, the sizable hole inside the main lake region of Fig. 8B corresponds to an island in the original image, which is neglected in the main lake region of Fig. 8A. Another distinction is that grouping in the maximum scheme is symmetrical in the sense that if pixel a can recruit pixel b , then b can recruit a as well. This is because effective weights are symmetrical, namely $W_{ij} = W_{ji}$ (see the algorithm). Because the maximum scheme appears to produce better results, it will be used in all of the following simulations.

To show the effects of parameters, we reduce the value of θ_p from 1200 in Fig. 8B to 1000. As a result, more regions are segmented, as shown in Fig. 8C where 23 segments plus a background are produced by the algorithm. Compared with Fig. 8B, the notable new segments include an open-theater-like region to the left of the main lake, and its nearby field region. The Lake image has been used in the study of Sarkar and Boyer (Sarkar and Boyer 1993a). As mentioned in Sect. 2.1, their approach is edge-based. The reader is encouraged to compare our results with theirs.

5.2.2 MRI images

The next image to test our algorithm is an MRI (magnetic resonance imaging) image of a human head, as shown in Fig. 9A. MRI images constitute a large class of medical images, and their automatic processing is of great practical value. This particular image, which we denote as Brain-1, is a midsagittal section, consisting of 257x257 pixels. Salient regions of this picture include the cerebral cortex, the cerebellum, the brainstem, the corpus callosum, the fornix (the bright stripe below the corpus callosum), the septum pellucidum (the region surrounded by the corpus callosum and the fornix), the extracranial soft tissue (the bright stripe on top of the head), the bone marrow (scattered stripes under the extracranial tissue), and several other structures (for the nomenclature see p. 318 of Kandel *et al.* 1991). For this image, a LEGION network of

257x257 oscillators is used, and $W_z = 25$ and $\theta_p = 800$. Figure 9B shows the result of one simulation by a gray map. The Brain-1 image is segmented into 21 regions, plus a background which is indicated by the black areas. Of particular interest are two parts of the brain: the upper part, and the brainstem with part of the spinal cord (to be called "brainstem" for short), parts of the extracranial tissue, and parts of the bone marrow. Other interesting segments include the neck part, the chin part, the nose part, and the vertebral segment.

Though it is useful to treat the brain as a whole in some circumstances, it may also be desirable to segment the brain into more detailed structures. To achieve this in LEGION, one can increase W_z . But in order not to produce too many regions, θ_p should usually be increased as W_z increases. To show the combined effects, Fig. 9C displays the result of another run with $W_z = 40$ and $\theta_p = 1000$, where Brain-1 is segmented to 25 regions plus a background. Now, the upper part of the brain is further segmented into the cerebral cortex, the cerebellum, the callosum/fornix region and its surrounding septum. Because of the higher W_z , regions in Fig. 9C tend to contain more background (compare, for example, the two brainstem regions). However, in the cortex segment in Fig. 9C, the noisy stripes actually have physical meanings: they tend to match with various fissures on the cerebral cortex. With the higher θ_p , some segments in Fig. 9B cannot generate any leaders and thus join the background.

The final segmentation uses another MRI image of a human head, shown in Fig. 10A. This image is denoted as Brain-2, consisting of 257x257 gray-level pixels. Brain-2 is a sagittal section through one eye. Salient regions of this picture include the cortex, the cerebellum, the lateral ventricle (the black hole within the cortex), the eye, the sinus (the black hole below the eye), the extracranial soft tissue, and the bone marrow. A LEGION network with 257x257 oscillators is used for the segmentation task. In the first simulation, $W_z = 20$ and $\theta_p = 800$, and Fig. 10B shows the result by a gray map. Brain-2 is segmented into 17 regions, plus a background which is indicated by black scattered areas. One can see from the figure that the entire brain forms a single segment. Other significant segments include the eye, the sinus, parts of the bone marrow, and parts of the extracranial tissue. The lateral ventricle is put into the background.

In order to generate finer structures, W_z is raised to 35 in the second simulation. As in Fig. 9, θ_p is increased to 1000. Fig. 10C shows the result of this simulation, where Brain-2 is segmented into 13 regions plus a background. As expected, the segments in Fig. 10B become further segmented or shrunk, and the background becomes more extensive. Worth mentioning is that the brain segment in Fig. 10B is segmented into three segments: one corresponding to the cortex and the other two corresponding to the cerebellum. Due to the increase of θ_p , the segments corresponding to the extracranial tissue and the marrow in Fig. 10B disappear in Fig. 10C.

In the segmentation experiments of this section, our goal was to illustrate the LEGION mechanism and the lateral potential effectiveness of derived algorithms. We did not attempt to produce best possible results by fine tuning of parameters. One can easily tell this by the simple rule of setting W_{ij} , the simple choice of $N(i)$, and the values of W_z and θ_p that have been used in the simulations. Therefore, better results can be expected by using more sophisticated schemes of choosing these parameters. Indeed, a more elaborate version of the LEGION algorithm has been applied to segment 3-dimensional MRI and CT (computerized tomography) images, and good segmentation results have been obtained (Shareef and Wang, in preparation).

6. Discussion

6.1 Further Remarks on LEGION Computation

In the simulations of Sect. 5, $N(i)$ is set to the eight nearest-neighbors of i . Larger $N(i)$'s entail more computations for determining leaders. But larger $N(i)$'s have more flexibility in specifying

the conditions for creating leaders, which tends to produce better results. Also, the order of pop-out of different segments is currently random. In some situations, however, it might be useful to influence the order of pop-out by some criteria, such as the size of each region. LEGION may incorporate different criteria by ordering leaders accordingly, e.g. by using the global inhibitor in different ways.

The main difference between our approach to image segmentation and other segmentation algorithms reviewed in Sect. 2 is that ours is neurocomputational, building on the strengths and the constraints of neural computation. Our approach relies on emergent behavior of LEGION to embody the computation involved in image segmentation. Methodologically, the computation is performed by a population of active agents - oscillators in this case - that are driven by pixels, whereas, in a typical segmentation algorithm, pixels are data to be processed by a central agent - the algorithm or the neural network trained as a pixel classifier. That LEGION is a massively parallel network of dynamical systems with mainly local coupling makes it particularly feasible for analog VLSI implementation, the success of which would be a major step towards real time processing of scene segmentation.

A thorny issue with scene segmentation is that often no unique answer exists. A house, for example, may be grouped into a single segment if viewed afar. The same house, if viewed nearby, may be broken into multiple segments including a door, a roof, windows, etc. This situation demands a flexible treatment of scene segmentation, i.e., a system should be able to easily generate multiple sets of segmentation, each of which should be reasonable. In LEGION, this flexibility is reflected to a certain degree by the effects of the parameters of W_z and θ_p , as discussed in Sect. 5. As noted there, both Fig. 9B and 9C are arguably reasonable results.

The LEGION network used so far has only one layer of oscillators. In Sect. 4, we mentioned that the oscillatory dynamics of one-layer LEGION has a limited segmentation capacity (see Fig. 6). It is interesting to note that the human perceptual system is also limited in simultaneously attending to the objects in a scene (Miller 1956). We expect that the ability of LEGION improves significantly when multiple layers are used in subsequent stages. This multistage processing provides a natural way out of this fundamental limitation. In multistage processing, each layer does not need to segregate more than several segments, and yet the system as a whole can segregate many more segments than the segmentation capacity - an idea reminiscent of chunking proposed by Miller (1956). When the number of segments in an image is greater than the segmentation capacity, one-layer LEGION will produce a number of segments (simple or congregate) up to the segmentation capacity (see Fig. 6). Congregate segments, however, can be further segmented with another layer of LEGION, whereas simple segments will not segment further. With multistage processing, the hierarchical system can provide results of both coarse- and fine-grain segmentation.

6.2 Biological Relevance

The relaxation-type oscillator used in LEGION is dynamically very similar to numerous other oscillators used in modeling neuronal behavior. Examples include the FitzHugh-Nagumo equations (FitzHugh 1961; Nagumo *et al.* 1962), and the Morris-Lecar model (Morris and Lecar 1981). These can all be viewed as simplifications of the Hodgkin-Huxley equations (Hodgkin and Huxley 1952). In (1), the variable x corresponds to the membrane potential of the neuron, and y corresponds to the channel activation or inactivation state variable which evolves on the slowest time scale. The reduction from a full Hodgkin-Huxley model to the two variable model is achieved by assuming that the other, faster, channel state variables are instantaneous. The dynamics of the lateral potential as given in (2) has properties similar to those of certain membrane channels and excitatory chemical synapses. The NMDA channel, for example, turns off on a slow time scale (Traub and Miles 1991). Moreover, with a sufficiently large input, a cell with these channels can be transformed from the excitatory to the oscillatory mode. We note that the lateral potential does

not act as a temporal integrator of all the input converging on its corresponding oscillator, but utilizes sharp nonlinearity as embodied by the outer Heaviside function in (2).

The theory of oscillatory correlation is consistent with the growing body of evidence that supports the existence of neural oscillations in the visual cortex and other brain regions. In the visual system, synchronous oscillations have been observed in cell recordings of the cat visual cortex (Eckhorn *et al.* 1988; Gray *et al.* 1989). These neural oscillations are stimulus-dependent, and range from 30 to 70 Hz, often referred to as *40 Hz oscillations*. Also, synchronous oscillations (locking with zero phase lag) occur across an extended brain region only if the stimulus constitutes a coherent object. These basic findings have been confirmed repeatedly in different brain regions and in different animal species (for reviews see Buzsáki *et al.* 1994 and Singer and Gray 1995).

The local excitatory connections assumed in LEGION conform with various lateral connections in the brain. Relating to the visual cortex, these excitatory connections, which link the excitatory elements of oscillators, could be interpreted as the horizontal connections in the visual cortex (Gilbert and Wiesel 1989; Gilbert 1992). It is known that horizontal connections originate from pyramidal cells, which are of excitatory type, and pyramidal cells are also the principal target of the horizontal connections. Furthermore, at the functional level, physiological recordings from monkeys suggest that motion-based visual segmentation may be processed in the primary visual cortex (Stoner and Albright 1992; Lamme *et al.* 1993). The global inhibitor (see Fig. 3) receives input from the entire oscillator network, and feeds back inhibition onto the network. It serves to segment multiple patterns simultaneously present in a visual scene, thus exerting a global coordination. Crick has suggested that part of the thalamus, the thalamic reticular complex in particular, may be involved in the global control of selective attention (Crick 1984). The thalamus is uniquely located in the brain: it receives input from and sends projections to almost the entire cortex. This suggestion and key anatomical and physiological properties of the thalamus prompt us to speculate that the global inhibitor might correspond to a neuronal group in the thalamus. The activity of the global inhibitor should be interpreted as the collective behavior of the neuronal group.

6.3 Figure-Ground Segregation

The dynamics proposed in this paper separates a scene into a number of major segments and a background, which corresponds to the rest of the scene. The major segments combine to form the foreground, whose corresponding oscillators are oscillatory until the input scene fades away. The oscillators corresponding to the background, after a brief beginning period, become excitable and stop oscillating. This dynamics effectively gets rid of noisy fragments without either prior smoothing or postprocessing of removing small regions, the methods often used in segmentation algorithms. With this dynamics, typical figure-ground segregation can be characterized as a special case, where only one major segment is allowed to be separated from the scene. In this sense, we claim that our dynamics also provides a potential solution to the problem of figure-ground segregation. We allow a foreground to include multiple segments, because this way both scene segmentation and figure-ground segregation are incorporated in a unified framework.

6.4 Future Topics

In the present study, we have not addressed the role of prior knowledge in image segmentation. For example, when people segment the images of Fig. 9A and Fig. 10A, they inevitably use their knowledge of human anatomy, which describes among other things the relative size and position of major brain regions. A more complete system of image segmentation must address this issue. Besides prior knowledge, many grouping principles outlined in Sect. 1 have not been incorporated into the system. One of the main future topics is to incorporate more grouping cues into the system. The global inhibitory mechanism will play a key role in overall

system coordination: it makes various factors compete with each other, and a final segment is formed because of strong binding within the segment.

Our study in this paper focuses exclusively on visual segmentation. It should be noted that neural oscillations occur in other modalities as well, including audition (Galambos *et al.* 1981; Ribary *et al.* 1991) and olfaction (Freeman 1978). Strikingly, these oscillations in different modalities show comparable frequencies. A recent study extended LEGION to deal with auditory scene segregation (Wang in press). With its computational properties and its biological relevance, the oscillatory correlation approach promises to provide a general neurocomputational theory for scene segmentation and perceptual organization.

Acknowledgments. The authors thank the two anonymous referees for their constructive comments. DLW was supported in part by the ONR grant N00014-93-1-0335, the NSF grant IRI-9423312, and the ONR YIP Award N00014-96-1-0676. DT was supported in part by the NSF grant DMS-9423796.

References

- Abeles, M. 1982. *Local cortical circuits*. Springer, New York.
- Abeles, M. 1991. *Corticonics: Neural circuits of the cerebral cortex*. Cambridge University Press, New York.
- Adams, R., and Bischof, L. 1994. Seeded region growing. *IEEE Trans. Pattern Anal. Machine Intell.* **16**, 641-647.
- Barlow, H. B. 1972. Single units and cognition: A neurone doctrine for perceptual psychology. *Percept.* **1**, 371-394.
- Buzsáki, G., Llinás, R., Singer, W., Berthoz, A., and Christen, Y. (ed.). 1994. *Temporal coding in the brain*. Springer-Verlag, Berlin Heidelberg.
- Crick, F. 1984. Function of the thalamic reticular complex: The searchlight hypothesis. *Proc. Natl. Acad. Sci. USA* **81**, 4586-4590.
- Eckhorn, R., *et al.* 1988. Coherent oscillations: A mechanism of feature linking in the visual cortex. *Biol. Cybern.* **60**, 121-130.
- FitzHugh, R. 1961. Impulses and physiological states in models of nerve membrane. *Biophys. J.* **1**, 445-466.
- Foresti, G., Murino, V., Regazzoni, C. S., and Vernazza, G. 1994. Grouping of rectilinear segments by the labeled Hough transform. *CVGIP: Image Understanding* **58**(3), 22-42.
- Freeman, W. J. 1978. Spatial properties of an EEG event in the olfactory bulb and cortex. *Electroencephalogr. Clin. Neurophysiol.* **44**, 586-605.
- Galambos, R., Makeig, S., and Talmachoff, P. J. 1981. A 40-Hz auditory potential recorded from the human scalp. *Proc. Natl. Acad. Sci. USA* **78**, 2643-2647.
- Geman, D., Geman, S., Graffigne, C., and Dong, P. 1990. Boundary detection by constrained optimization. *IEEE Trans. Pattern Anal. Machine Intell.* **12**, 609-628.
- Gilbert, C. D. 1992. Horizontal integration and cortical dynamics. *Neuron* **9**, 1-13.
- Gilbert, C. D., and Wiesel, T. N. 1989. Columnar specificity of intrinsic horizontal and corticocortical connections in cat visual cortex. *J. Neurosci.* **9**, 2432-2442.
- Gove, A., Grossberg, S., and Mingolla, E. in press. Brightness perception, illusory contours, and corticogeniculate feedback. *Visual Neurosci.*
- Gray, C. M., König, P., Engel, A. K., and Singer, W. 1989. Oscillatory responses in cat visual cortex exhibit inter-columnar synchronization which reflects global stimulus properties. *Nature* **338**, 334-337.
- Grossberg, S., and Mingolla, E. 1985. Neural dynamics of perceptual grouping: Textures, boundaries, and emergent computations. *Percept. Psychophys.* **38**, 141-171.
- Grossberg, S., and Wyse, L. 1991. A neural network architecture for figure-ground separation of connected scenic figures. *Neural Net.* **4**, 723-742.
- Gurari, E. M., and Wechsler, H. 1982. On the difficulties involved in the segmentation of pictures. *IEEE Trans. Pattern Anal. Machine Intell.* **4**(3), 304-306.
- Haralick, R. M. 1979. Statistical and structural approaches to texture. *Proc. IEEE* **67**, 786-804.
- Haralick, R. M., and Shapiro, L. G. 1985. Image segmentation techniques. *Comput. Graphics Image Process.* **29**, 100-132.
- Hodgkin, A. L., and Huxley, A. F. 1952. A quantitative description of membrane current and its application to conduction and excitation in nerve. *J. Physiol. (Lond.)* **117**, 500-544.
- Horowitz, S. L., and Pavlidis, T. 1976. Picture segmentation by a tree traversal algorithm. *J. ACM* **23**, 368-388.

- Kandel, E. R., Schwartz, J. H., and Jessell, T. M. 1991. *Principles of neural science*, 3rd ed. Elsevier, New York.
- Koffka, K. 1935. *Principles of Gestalt psychology*. Harcourt, New York.
- Koh, J., Suk, M., and Bhandarkar, S. M. 1995. A multilayer self-organizing feature map for range image segmentation. *Neural Net.* **8**, 67-86.
- Kohler, R. 1981. A segmentation system based on thresholding. *Comput. Graphics Image Process.* **15**, 319-338.
- Kohonen, T. 1995. *Self-organizing maps*. Springer, Berlin Heidelberg.
- Lamme, V. A. F., van Dijk, B. W., and Spekreijse, H. 1993. Contour from motion processing occurs in primary visual cortex. *Nature* **363**, 541-543.
- Liou, S. P., Chiu, A. H., and Jain, R. C. 1991. A parallel technique for signal-level perceptual organization. *IEEE Trans. Pattern Anal. Machine Intell.* **13**, 317-325.
- Manjunath, B. S., and Chellappa, R. 1993. A unified approach to boundary perception: Edges, textures, and illusory contours. *IEEE Trans. Neural Net.* **4**, 96-108.
- Miller, G. A. 1956. The magical number seven, plus or minus two: Some limits on our capacity for processing information. *Psychol. Rev.* **63**, 81-97.
- Milner, P. M. 1974. A model for visual shape recognition. *Psychol. Rev.* **81**(6), 521-535.
- Mohan, R., and Nevatia, R. 1992. Perceptual organization for scene segmentation and description. *IEEE Trans. Pattern Anal. Machine Intell.* **14**, 616-635.
- Morris, C., and Lecar, H. 1981. Voltage oscillations in the barnacle giant muscle fiber. *Biophys. J.* **35**, 193-213.
- Mozer, M. C., Zemel, R. S., Behrmann, M., and Williams, C. K. I. 1992. Learning to segment images using dynamic feature binding. *Neural Comp.* **4**, 650-665.
- Murata, T., and Shimizu, H. 1993. Oscillatory binocular system and temporal segmentation of stereoscopic depth surfaces. *Biol. Cybern.* **68**, 381-390.
- Nagumo, J., Arimoto, S., and Yoshizawa, S. 1962. An active pulse transmission line simulating nerve axon. *Proc. IRE* **50**, 2061-2070.
- Ribary, U., *et al.* 1991. Magnetic field tomography of coherent thalamocortical 40-Hz oscillations in humans. *Proc. Natl. Acad. Sci. USA* **88**, 11037-11041.
- Rock, I., and Palmer, S. 1990. The legacy of Gestalt psychology. *Sci. Am.* **263**, 84-90.
- Sarkar, S., and Boyer, K. L. 1993a. Integration, inference, and management of spatial information using Bayesian networks: Perceptual organization. *IEEE Trans. Pattern Anal. Machine Intell.* **15**, 256-274.
- Sarkar, S., and Boyer, K. L. 1993b. Perceptual organization in computer vision: a review and a proposal for a classificatory structure. *IEEE Trans. Syst. Man Cybern.* **23**, 382-399.
- Schalkoff, R. 1992. *Pattern recognition: Statistical, structural and neural approaches*. Wiley & Sons, New York.
- Schillen, T. B., and König, P. 1994. Binding by temporal structure in multiple feature domains of an oscillatory neuronal network. *Biol. Cybern.* **70**, 397-405.
- Sejnowski, T. J., and Hinton, G. E. 1987. Separating figure from ground with a Boltzmann machine. In *Vision, brain, and cooperative computation*, M. A. Arbib, and A. R. Hanson, ed., pp. 703-724. MIT Press, Cambridge MA.
- Singer, W. 1993. Synchronization of cortical activity and its putative role in information processing and learning. *Ann. Rev. Physiol.* **55**, 349-374.
- Singer, W., and Gray, C. M. 1995. Visual feature integration and the temporal correlation hypothesis. *Ann. Rev. Neurosci.* **18**, 555-586.

- Somers, D., and Kopell, N. in press. Waves and synchrony in networks of oscillators of relaxation and non-relaxation type. *Physica D*.
- Sompolinsky, H., Golomb, D., and Kleinfeld, D. 1991. Cooperative dynamics in visual processing. *Phys. Rev. A* **43**, 6990-7011.
- Sporns, O., Tononi, G., and Edelman, G. M. 1991. Modeling perceptual grouping and figure-ground segregation by means of active re-entrant connections. *Proc. Natl. Acad. Sci. USA* **88**, 129-133.
- Stoner, G. R., and Albright, T. D. 1992. Neural correlates of perceptual motion coherence. *Nature* **358**, 412-414.
- Terman, D., and Wang, D. L. 1995. Global competition and local cooperation in a network of neural oscillators. *Physica D* **81**, 148-176.
- Traub, R. D., and Miles, R. 1991. *Neuronal networks in the hippocampus*. Cambridge University Press, New York.
- von der Malsburg, C. 1981. The correlation theory of brain function. Internal Report 81-2, Max-Planck-Institute for Biophysical Chemistry.
- von der Malsburg, C., and Buhmann, J. 1992. Sensory segmentation with coupled neural oscillators. *Biol. Cybern.* **54**, 29-40.
- von der Malsburg, C., and Schneider, W. 1986. A neural cocktail-party processor. *Biol. Cybern.* **54**, 29-40.
- Wang, D. L. 1993a. Modeling global synchrony in the visual cortex by locally coupled neural oscillators. In *Proc. of 15th Ann. Conf. Cognit. Sci. Soc.*, pp. 1058-1063. Boulder CO.
- Wang, D. L. 1993b. Pattern recognition: Neural networks in perspective. *IEEE Expert* **8**, 52-60, August.
- Wang, D. L. 1995. Emergent synchrony in locally coupled neural oscillators. *IEEE Trans. Neural Net.* **6**(4), 941-948.
- Wang, D. L. in press. Primitive auditory segregation based on oscillatory correlation. *Cognit. Sci.*
- Wang, D. L., Buhmann, J., and Malsburg, C. v. d. 1990. Pattern segmentation in associative memory. *Neural Comp.* **2**, 95-107. Reprinted in Olfaction, J.L. Davis and H. Eichenbaum, ed. Cambridge MA: MIT Press, pp. 213-224, 1991.
- Wang, D. L., and Terman, D. 1995a. Locally excitatory globally inhibitory oscillator networks. *IEEE Trans. Neural Net.* **6**(1), 283-286.
- Wang, D. L., and Terman, D. 1995b. Image segmentation based on oscillatory correlation. In *Proc. of World Congress on Neural Net.*, pp. II.521-525.
- Wang, D. L., and Terman, D. 1996. Image segmentation based on oscillatory correlation. Tech. Rep. 19, OSU Center for Cognitive Science.
- Wertheimer, M. 1923. Untersuchungen zur Lehre von der Gestalt, II. *Psychol. Forsch.* **4**, 301-350.
- Zucker, S. W. 1976. Region growing: Childhood and adolescence. *Comput. Graphics Image Process.* **5**, 382-399.

Figure Caption

Figure 1. A caricature of an image with three objects that appears on a noisy background. The noiseless caricature is adapted from Terman and Wang (1995).

Figure 2. Nullclines and orbits of a single oscillator (We thank S. Campbell for making this figure). **A.** If $I > 0$ and $H = 1$, the oscillator is enabled. The periodic orbit is shown with a bold curve, and its direction of motion is indicated by the arrowheads. The left and the right branches of the x -nullcline are labeled as L and R , respectively. LK and RK indicate the left and the right knees of the cubic, respectively. **B.** If $I \leq 0$ and $H = 1$, the oscillator is excitable. The fixed point P_I on the left branch of the cubic is asymptotically stable.

Figure 3. Architecture of a two dimensional LEGION network with four nearest-neighbor coupling. An oscillator is indicated by an open circle, and the global inhibitor is indicated by the filled circle.

Figure 4. **A** An image composed of three patterns on a noisy background. The image is mapped to a 50×50 LEGION network. Each square corresponds to an oscillator. If a square is entirely covered, the corresponding oscillator receives external input; otherwise, the oscillator receives no external input. In the figure, B-E correspond to the case with the inclusion of the lateral potential, whereas F-J correspond to the case without the lateral potential. **B** A snapshot at the beginning of dynamic evolution. **C-E** Snapshots subsequently taken shortly after **B**. **F** A snapshot at the beginning of dynamic evolution for the case without the lateral potential. **G-J** Snapshots subsequently taken shortly after **F**.

Figure 5. Temporal evolution of every stimulated oscillator. The upper three traces show the combined x activities of the three oscillator blocks representing the three corresponding patterns indicated by their respective labels. The fourth trace shows the temporal activities of the loners, and the bottom trace shows the activity of the global inhibitor. The ordinates indicate the normalized activity of an oscillator or the inhibitor. The simulation took 9,000 integration steps.

Figure 6. **A** An image composed of nine patterns mapped to a 30×30 LEGION network. See the legend of Fig. 4 for explanations. **B** The image in **A** is corrupted by 10% noise. **C** A snapshot of network activity at the beginning of dynamic evolution. **D-F** Snapshots subsequently taken shortly after **C**.

Figure 7. **A** A gray-level image consisting of 160×160 pixels (courtesy of K. Boyer). **B-G** Segments popped out subsequently from the network shortly after the LEGION algorithm is executed. (We thank E. Cesmeli for his assistance in making this display)

Figure 8. **A** A gray map showing the result of segmenting Fig. 7A. The algorithm produces 16 segments plus a background. **B** The result of another segmentation using maximization to compute S_i . The algorithm produces 17 segments plus a background. **C** The result of another segmentation similar to **B** but with a different value for θ_p . The system produces 23 segments plus a background. The algorithm was run for 1,000 steps for every case.

Figure 9. **A** A gray-level image consisting of 257×257 pixels (courtesy of N. Shareef). **B** A gray map showing the result of segmenting the image by a 257×257 LEGION network. The system produces 21 segments plus a background. **C** The result of another segmentation with different values of W_z and θ_p . The system produces 25 segments plus a background. The algorithm was run for 1,200 steps in both **B** and **C**.

Figure 10. **A** A gray-level image consisting of 257×257 pixels (courtesy of N. Shareef). **B** A gray map showing the result of segmenting the image by a 257×257 LEGION network. The system produces 17 segments plus a background. **C** The result of another segmentation with different values of W_z and θ_p . The system produces 13 segments plus a background. The algorithm was run for 1,200 steps in both **B** and **C**.

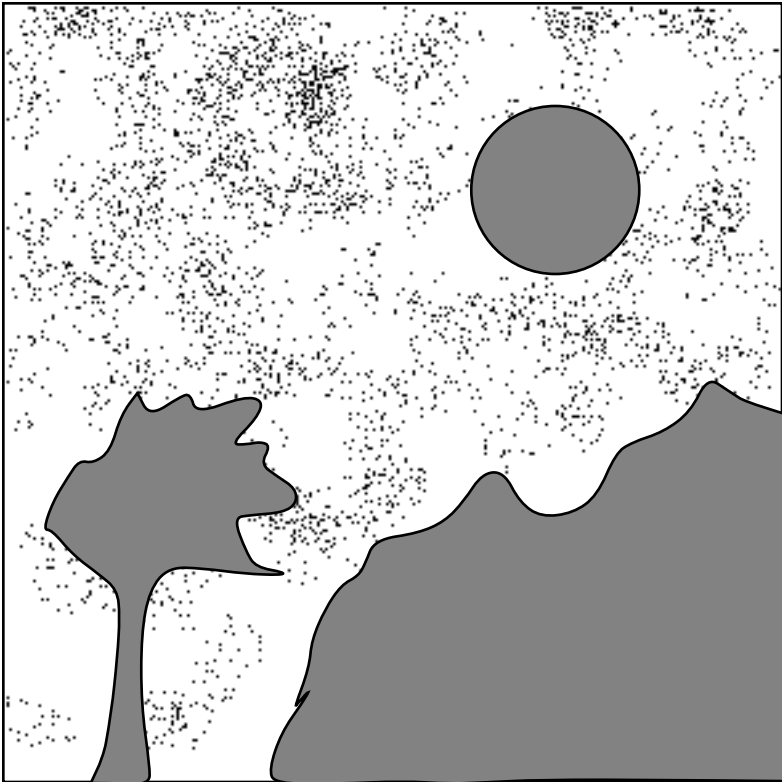


Figure 1

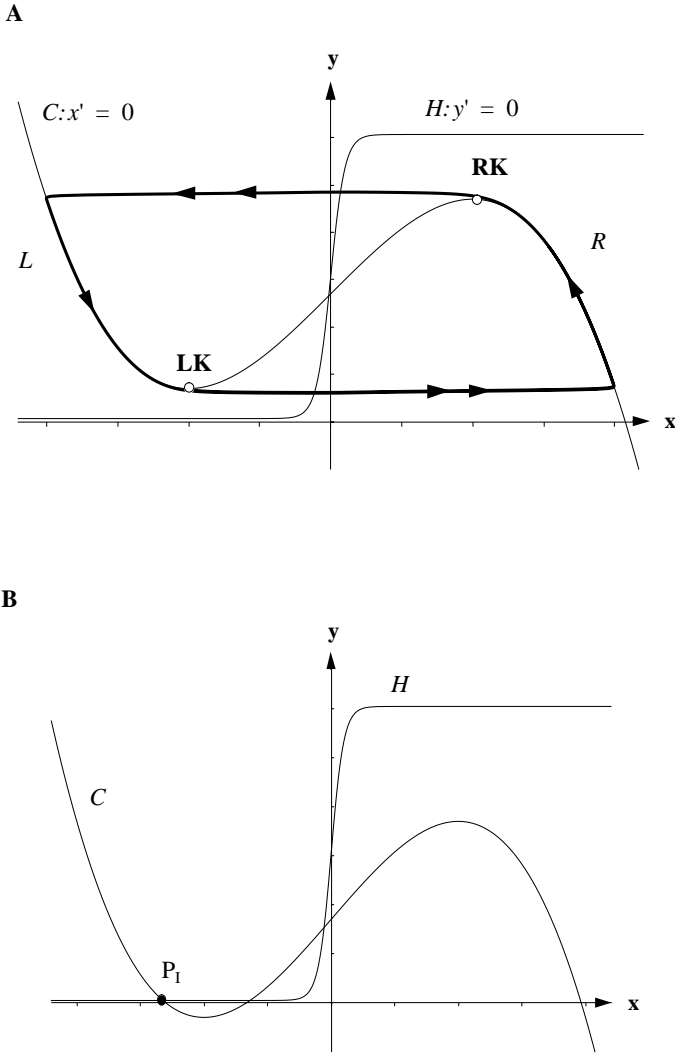


Figure 2

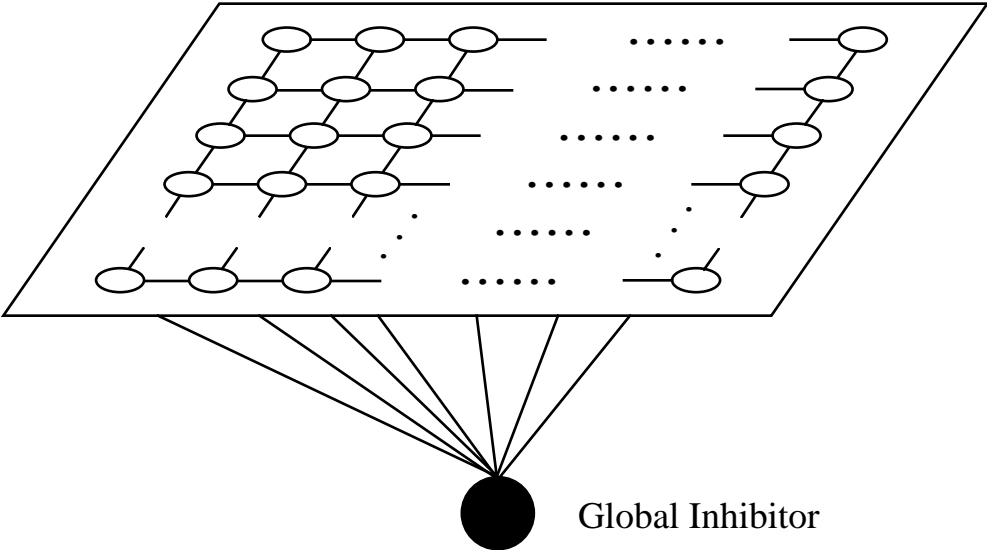
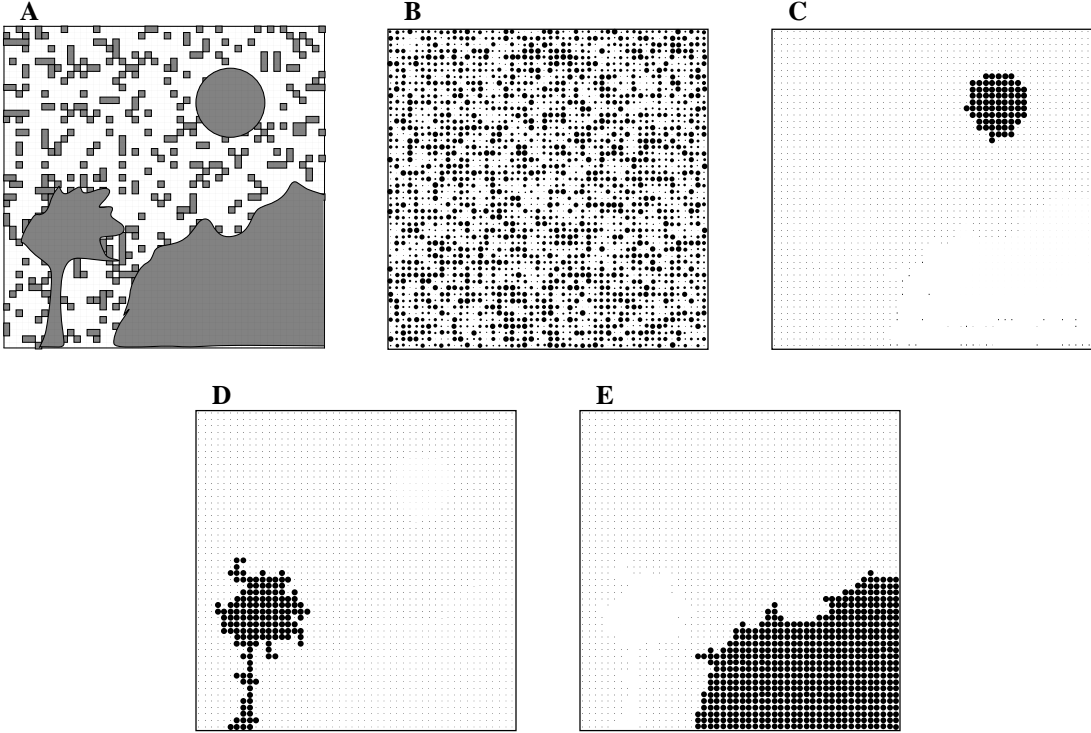


Figure 3

With Lateral Potential



Without Lateral Potential

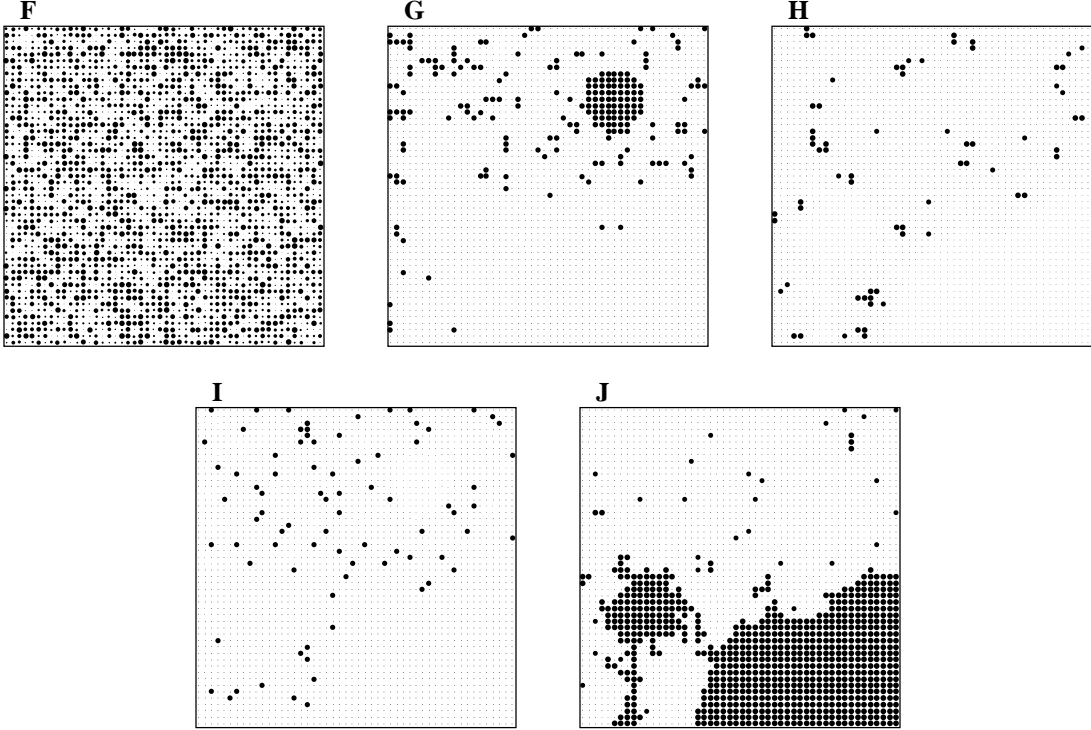


Figure 4

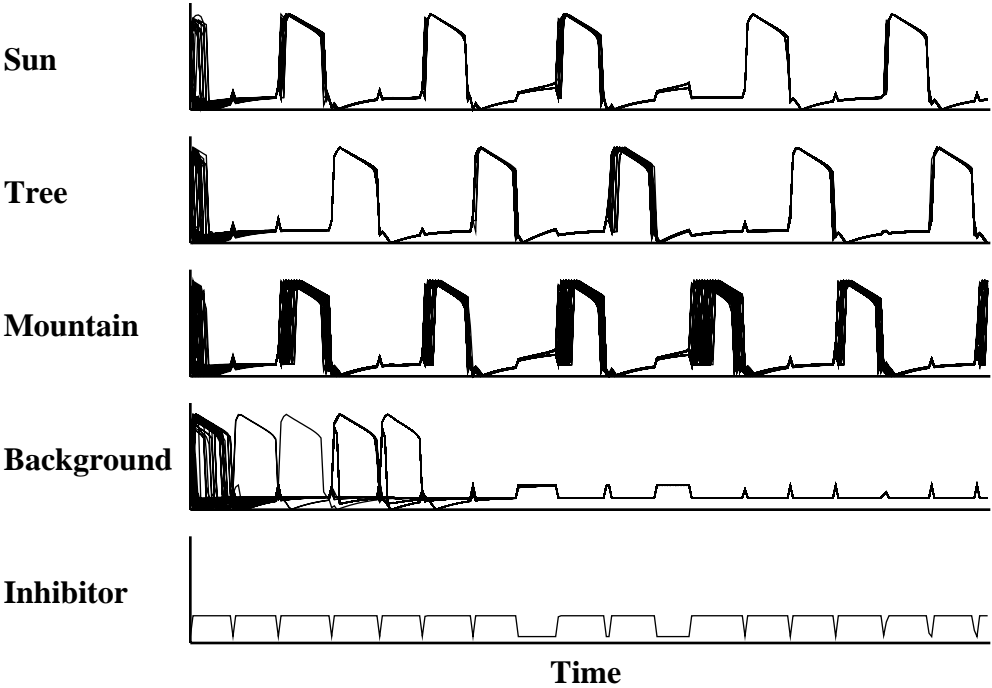


Figure 5

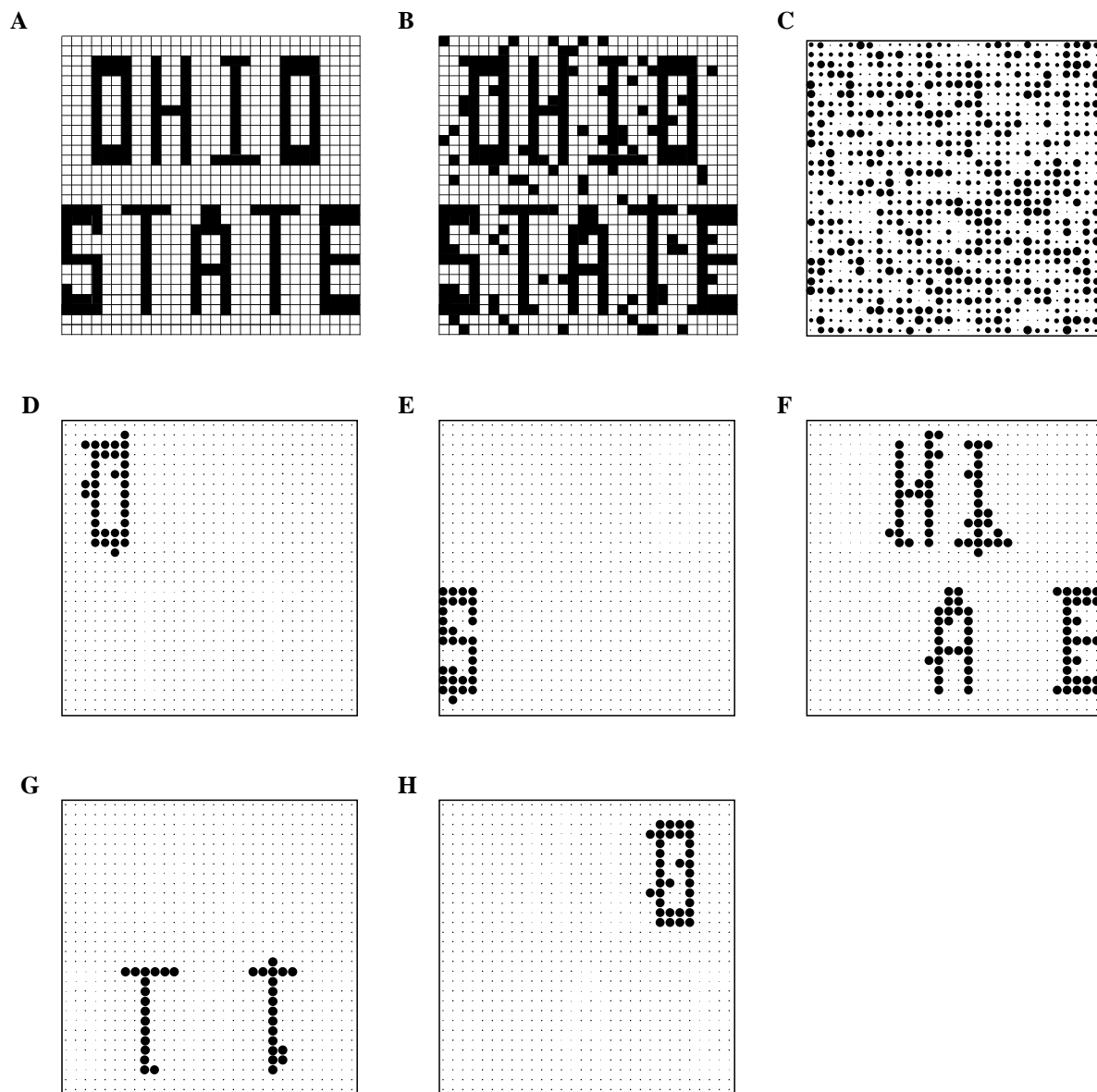


Figure 6

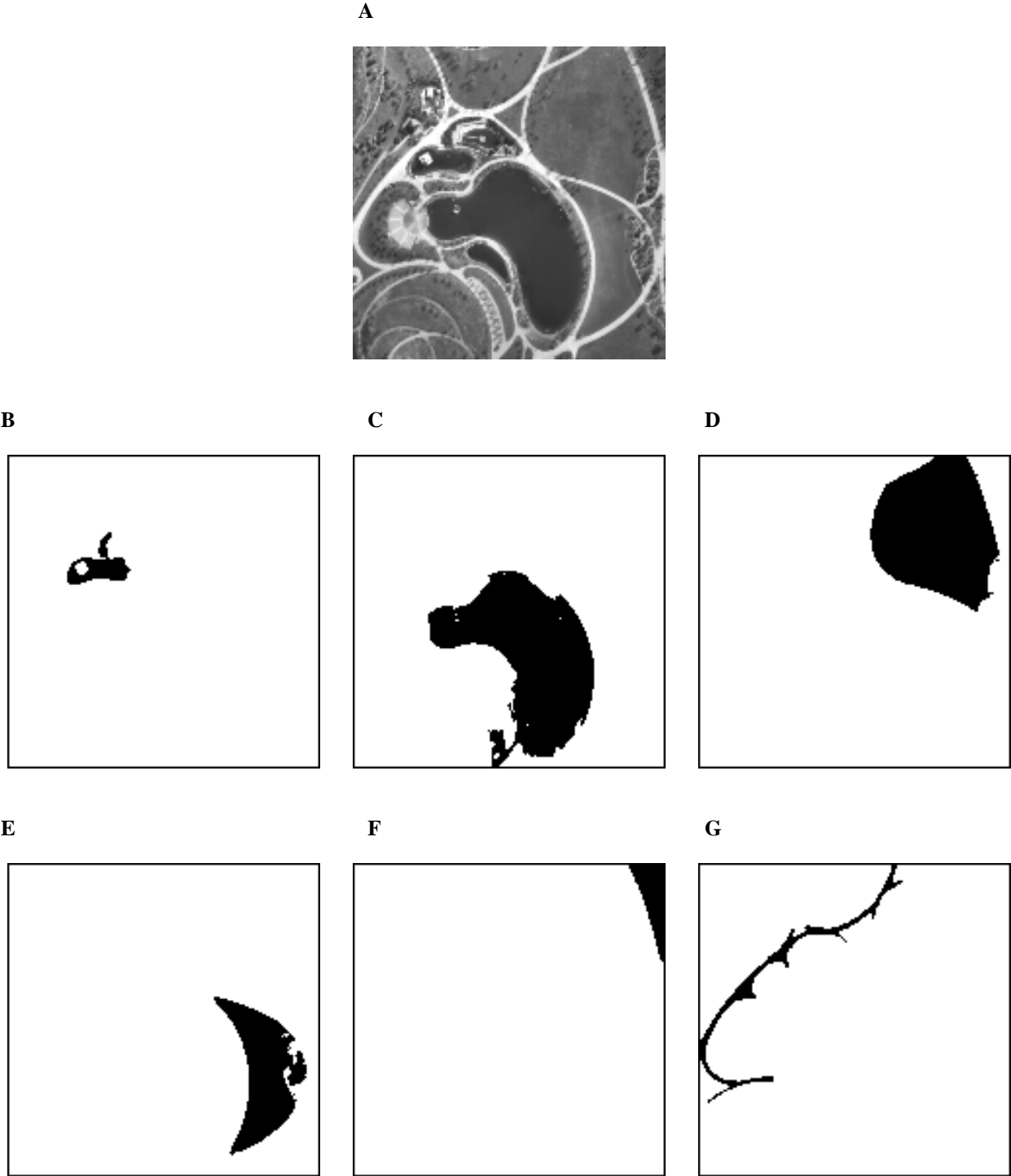


Figure 7

A



B



C



Figure 8

A



B

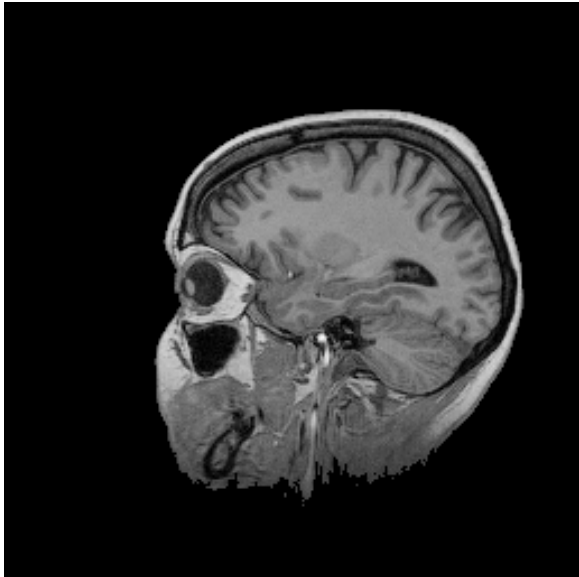


C

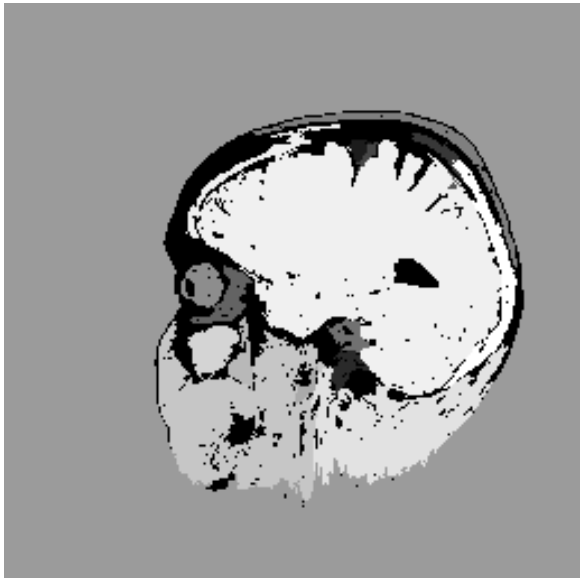


Figure 9

A



B



C

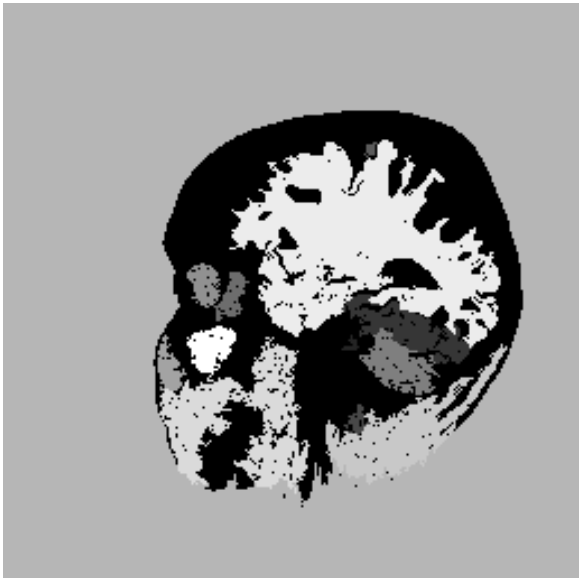


Figure 10